First-principles investigation of Ge doping effects on the structural, electronic and magnetic properties in antiperovskite Mn_3CuN

2010 J. Phys.: Condens. Matter 22 206003

(http://iopscience.iop.org/0953-8984/22/20/206003)

J. Phys.: Condens. Matter **22** (2010) 206003 (5pp) doi:10.1088/0953-8984/22/20/206003

First-principles investigation of Ge doping effects on the structural, electronic and magnetic properties in antiperovskite Mn_3CuN

L Hua[1], **L Wang and L F Chen**

Department of Physics, Nanjing Normal University, Nanjing 210097, People's Republic of China

E-mail: pjsd@163.com

Received 11 January 2010, in final form 4 March 2010
Published 26 April 2010
Online at stacks.iop.org/JPhysCM/22/206003

Abstract

We have investigated the structural, electronic, and magnetic properties of $Mn_3Cu_{1-x}Ge_xN$ ($x = 0, 0.125, 0.25$) using first-principles density-functional theory within the generalized gradient approximation (GGA) + U schemes. The crystal structure of the compounds is a tetragonal crystal for $x = 0$ while it is a cubic crystal for $x = 0.125, 0.25$. The unit cell volume increases as the Ge doping increases. Our GGA + U calculations give a metallic ground state from $x = 0$ to 0.25 in agreement with experiments. The magnetic structure for $x = 0$ is found to be the ferromagnetic state while for $x = 0.125, 0.25$ it is the Γ^{5g}-type antiferromagnetic state. From the density of states (DOS), the coupling between Ge 4p and Mn 3d is the main reason for magnetic transition in $Mn_3Cu_{1-x}Ge_xN$.

(Some figures in this article are in colour only in the electronic version)

1. Introduction

Most solids exhibit thermal expansion, i.e. their lattice parameters increase on heating under constant pressure. A very limited number of materials, however, contract on heating and show negative thermal expansion (NTE) [1–3]. There has been considerable interest in these NTE materials because of the variety of their potential applications. NTE materials can compensate or control (positive) thermal expansion of materials by forming composites, which have been widely used as, for example, high-precision (zero expansion) optical and machinery parts [4, 5]. An important mechanism of NTE is the magnetovolume effect (MVE). With decreasing temperature (T), the volume can be expanded gradually by changing the amplitude of the magnetic moment. This MVE of itinerant electron systems has been investigated since the discovery of extraordinarily small thermal expansion in Invar alloys [6].

Antiperovskite manganese nitrides Mn_3 AN, where A is a metal or a semiconducting element (A = Zn, Ge, etc), are well known for their large MVE [7–10]. The A atom occupies a cubic lattice corner position, whereas the Mn and N atoms are located at the face-centered and body-centered positions, as shown in figure 1. So far, all the MVEs reported in Mn_3AN members are associated with first-order phase transitions and the lattice volume sudden increasing with decreasing temperature. This is why Mn_3AN has not been considered as a practical NTE material to date.

Recently, Takenaka and Takagi reported that the MVE is broadened against T in $Mn_3Cu_{1-x}Ge_xN$ and leads to a giant negative thermal expansion coefficient [11]. This system shows three different characteristic behaviors of the MVE as a function of Ge concentration x. (i) Mn_3CuN shows the paramagnetic to ferromagnetic transition at T_c = 143 K accompanied by a cubic-to-tetragonal structural phase transition. At the transition, the volume change is negligibly small. (ii) At $x = 0.15$, the ferromagnetic and structural phase transition takes place at $T_c \sim 100$ K and linear thermal expansion $\Delta L/L$ rapidly increases at that temperature with decreasing T. (iii) With increasing x ($x = 0.3, 0.4, 0.5, 0.55$), the magnetic transition is from paramagnetic to

[1] Author to whom any correspondence should be addressed.

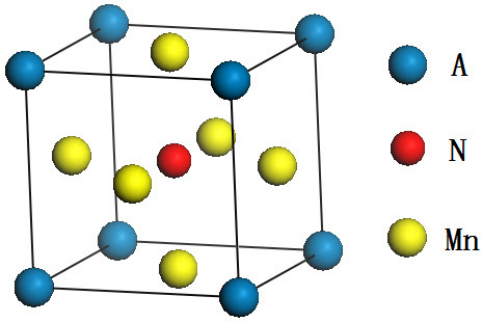

Figure 1. The stoichiometric antiperovskite Mn_3AN unit cell. The blue, yellow, and red spheres denote the A, Mn, and N atoms, respectively.

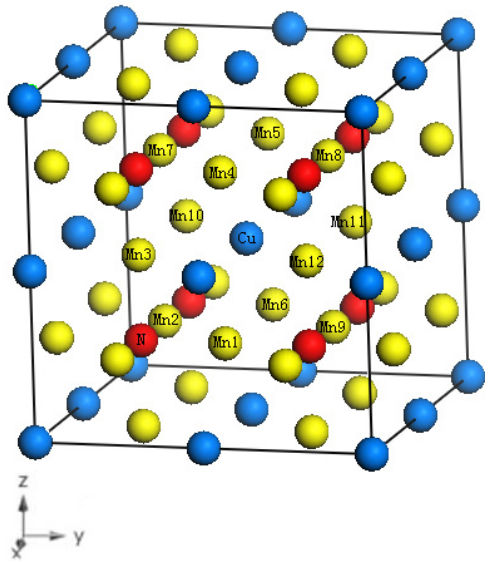

Figure 2. Mn_3CuN $2 \times 2 \times 2$ supercell consists of 40 atoms with three inequivalent Mn sites designated as Mn1, Mn2, and Mn3, respectively. Nearest-neighbor Mn of Cu are designated as Mn1–Mn12.

antiferromagnetic and the increase of $\Delta L/L$ occurs over a broader range of T. They suspected that Ge dopants give rise to a strong local disorder, which might give rise to a relaxor-like behavior as in *relaxor ferroelectrics* [12] or *relaxor ferromagnets*, resulting in MVE [13]. Iikubo *et al* [14] performed experiments on $Mn_3Cu_{1-x}Ge_xN$ and found that the compound undergoes a paramagnetic to antiferromagnetic change while remaining structurally unchanged in $x = 0.15$ where MVE appears with the temperature decreasing. They also calculated the magnetism and concluded that $Mn_3Cu_{1-x}Ge_xN$ ($x \geqslant 0.15$) are Γ^{5g}-type antiferromagnetic cubic phase.

Generally speaking, $Mn_3Cu_{1-x}Ge_xN$ antiperovskite materials of itinerant electron systems are well known for their large MVEs. Their volumes show a pronounced increase with decreasing temperature at the first-order magnetic and structural transition, and they exhibit the Γ^{5g}-type antiferromagnetic cubic structure below the phase transition temperature. In order to understand the Ge doping effects on the magnetic properties and structure transition in $Mn_3Cu_{1-x}Ge_xN$, we perform density-functional electronic structure calculations on $Mn_3Cu_{1-x}Ge_xN$ ($x = 0$, 0.125, 0.25) and clarify the role of germanium in the mechanism of magnetic transition.

2. Computational details

Our calculations are performed using the first-principles simulation code VASP [15–18]. The total energy is calculated using the projector augmented-wave (PAW) method [19, 20] together with the Perdew and Wang exchange–correlation functional (PW91) [21] in the generalized gradient approximation (GGA). The local spin density approximation (LSDA) and GGA are known to fail in the description of the electronic properties of early transition metal (TM) compounds, as the electron self-interaction error, always present in these formulations, becomes significant for electrons in the well-localized TM d levels. Thus we have employed the DFT + U [22–25] methodology which is able to significantly improve predictions of phase stability and magnetic structure. We use here the simple formulation by Liechtenstein *et al* and Dudarev *et al*, where a single parameter U_{eff} determines an orbital-dependent correction to the density-functional theory (DFT) energy. U_{eff} is generally expressed as the difference between two parameters, the Hubbard U, which is the Coulomb-energetic cost of placing two electrons at the same site, and an approximation of the Stoner exchange parameter J, which is almost constant at 1 eV. The value of U_{eff} is 2.2 eV in our calculations. 3d4s for Mn, 3d4s for Cu, 4s4p for Ge, 2s2p for N are treated as valence orbitals in the calculations. Electronic wavefunctions are expanded with plane waves up to an energy cutoff (E_{cut}) of 400 eV. Brillouin zone sampling is performed on a Monkhorst–Pack (MP) mesh [26] of $4 \times 4 \times 4$. Bulk and Ge doping calculations are performed in a $2 \times 2 \times 2$ supercell with 40 atoms. Forces on atoms are calculated and atoms are allowed to relax using a conjugate gradient technique until their residual forces have converged to less than 0.01 eV Å^{-1}. For $Mn_3Cu_{1-x}Ge_xN$, we substitute one Cu atom with Ge to form $Mn_3Cu_{0.875}Ge_{0.125}N$ and two Cu atoms to form $Mn_3Cu_{0.75}Ge_{0.25}N$.

3. Results and discussion

3.1. Structure relaxation

We have constructed a $2 \times 2 \times 2$ supercell consisting of 40 atoms with three inequivalent Mn sites at Mn1(0.75, 0.5, 0.25), Mn2(0.5, 0.25, 0.25), and Mn3(0.75, 0.25, 0.5) positions for the bulk sample, as shown in figure 2. For $Mn_3Cu_{0.875}Ge_{0.125}N$, there is only one inequivalent Ge site substitution at Cu(0.5, 0.5, 0.5) while for $Mn_3Cu_{0.75}Ge_{0.25}$, there are three kinds of inequivalent Ge site substitutions which are along the [100], [101], and [111] directions, respectively. We calculate the total energy of three kinds of inequivalent Ge site substitutions and find that the supercell with Ge site substitution along the [100] direction owns the lowest total energy. Thus we select this kind of Ge site substitution as our *ab initio* calculations.

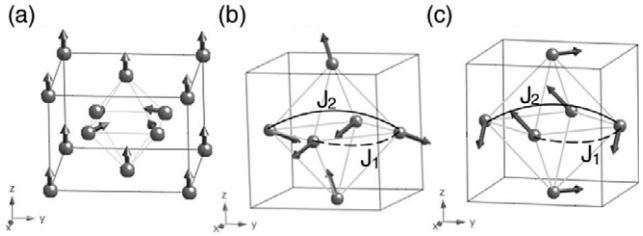

Figure 3. (a) Magnetic structure of Mn_3CuN. (b) Γ^{4g}-type AFM cubic structure. (c) Γ^{5g}-type AFM cubic structure. Cu, Ge, and N atoms are omitted for simplicity [14].

Mn_3CuN has a tetragonal crystal structure (space group: $P4/mmm$) and the magnetic ordering vector $\mathbf{q} = (\frac{1}{2}\ \frac{1}{2}\ 0)$, indicating that the magnetic unit cell becomes doubled along the a and b axes at low temperatures. The magnetic structure of Mn_3CuN is shown in figure 3(a). The Mn moments on the $z = 0.5$ plane have a square configuration and a small ferromagnetic component along the c axis. The Mn moments on the $z = 0$ plane have a parallel configuration. Ge doping samples have a cubic structure (space group: $Pm\bar{3}m$) and magnetic ordering vector $\mathbf{q} = (0\ 0\ 0)$. On the basis of these conditions, three possible models have been proposed by Fruchart and Bertaut [7]. They considered a spin Hamiltonian with superexchange interactions among Mn ions up to the second nearest neighbors. The eigenstates consist of a collinear ferromagnetic (FM) structure and two triangular antiferromagnetic (AFM) structures, where Mn moments point 120° away from each other. The direction of Mn moments cannot be determined within the above consideration. The real spin structures are determined to be represented by the three models that are allowed by linear combination of the basis vectors of irreducible representations for the $Pm\bar{3}m$ group with $\mathbf{q} = (0\ 0\ 0)$. One is an FM structure belonging to the Γ^{4g}-type irreducible representation, and two are AFM structures belonging to Γ^{4g}-type and Γ^{5g}-type, respectively. Figures 3(b) and (c) show Γ^{4g}-type AFM and Γ^{5g}-type AFM magnetic structures. The ordering patterns imply that nearest-neighbor J1 and next-nearest-neighbor J2 are AFM and FM, respectively, and show the effect of the geometrical frustration originating from J1.

Table 1 lists calculated structural parameters, total magnetic moments, and total energy for $Mn_3Cu_{1-x}Ge_xN$ ($x = 0, 0.125, 0.25$). From table 1, we can see that the total energy of the Mn_3CuN FM state is lower than that of the Γ^{4g}, Γ^{5g} AFM state, while the $Mn_3Cu_{1-x}Ge_xN$ ($x = 0.125, 0.25$) Γ^{5g} AFM state is lowest. These results are in agreement with Iikubo *et al* [14]. The crystal structure of the compounds for $x = 0$ is tetragonal while $x = 0.125, 0.25$ are cubic. For $x = 0$ the unit cell volume is 58.258 (Å^3) which is consistent with experiment 58.950 (Å^3) [27]. The cell volume increases with x increasing. The systematic increase of the cell volume with increasing x can be explained by the ionic radius of Ge being larger than that of Cu in the compounds. The average nearest-neighbor bond distances of $d_{\langle N-Mn\rangle}$, $d_{\langle Mn-Mn\rangle}$, $d_{\langle Cu-Mn\rangle}$, and $d_{\langle Ge-Mn\rangle}$ increase with x increasing.

Table 1. Calculated structural parameters, total magnetic moments, and total energy for $Mn_3Cu_{1-x}Ge_xN$ ($x = 0, 0.125, 0.25$) (experiment values are given in the parenthesis).

Composition x	0	0.125	0.25
a (Å)	3.890(3.912)	3.903	3.907
b (Å)	3.890(3.912)	3.903	3.907
c (Å)	3.850(3.852)	3.903	3.907
V (Å^3)	58.258(58.950)	59.501	59.639
$d_{\langle N-Mn\rangle}$ (Å)	1.925	1.952	1.954
$d_{\langle Mn-Mn\rangle}$ (Å)	2.737	2.760	2.763
$d_{\langle Cu-Mn\rangle}$ (Å)	2.737	2.760	2.763
$d_{\langle Ge-Mn\rangle}$ (Å)	—	2.760	2.763
μ_T (μ_B/f.u.)	10.23	0.00	0.00
E(FM) (eV)	−313.74	−315.37	−317.28
E (Γ^{4g}AFM) (eV)	−312.72	−315.89	−318.34
E (Γ^{5g}AFM) (eV)	−312.86	−315.92	−318.42

3.2. Electronic structure

We know that the nitrogen atom in the Mn_3CuN structure, with 2p orbital electrons, can hybridize with the 180° near-neighbor Mn 3d e_g electrons. Complementarily, near-neighbor Mn–Mn interactions are provided by orthogonal t_{2g} electrons along the edges of the Mn octahedra. Thus both direct Mn–Mn and indirect Mn–N–Mn interactions are present. According to the Goodenough–Anderson–Kanamori rules [28], in 180° Mn–N–Mn interactions, Mn cations with under half-filled d shell, are FM, whereas Mn–Mn interactions are AFM. So there are two kinds of magnetic interactions which are 180° Mn–N–Mn FM interactions and 90° Mn–Mn AFM interactions in Mn_3CuN. From table 1, we can see that nearest-neighbor $d_{\langle N-Mn\rangle}$ and $d_{\langle Mn-Mn\rangle}$ increase with Ge doping while the increasing distance of $d_{\langle N-Mn\rangle}$ (0.027 Å) is larger than $d_{\langle Mn-Mn\rangle}$ (0.023 Å) in $x = 0.125$. This means that 180° Mn–N–Mn FM interactions become weak while 90° Mn–Mn AFM interactions become strong. At $x = 0.125$, the Mn–N–Mn FM interactions are overcome by the Mn–Mn AFM interactions in the compounds which result in the AFM state. The calculated total magnetic moments (μ_T) for $Mn_3Cu_{1-x}Ge_xN$ are also listed in table 1. The magnetic structures for $x = 0$ are found to be in the FM state while for $x = 0.125, 0.25$ they are in the AFM state which is consistent with experiments.

Our GGA + U calculations give a metallic ground state from $x = 0$ to 0.25 in $Mn_3Cu_{1-x}Ge_xN$, as shown in figure 4, which is in agreement with experiments [14]. In figure 4, we show the calculated total density of states (DOS) and partial Mn 3d, Cu 4s, Ge 4p, and N 2p DOS for different x. For our discussion of the DOS, we are limited to an energy window of −7.5 to about 0.5 eV. For Mn_3CuN, the composition $x = 0$ (see figure 4(a)), We can see that the N 2p hybridizes mainly with the Mn 3d from −7.5 to −4 eV while Cu 4s is from −5 to −3 eV. At the Fermi level E_f, Cu 4s and N 2p state are small, so the DOS at E_f are mainly a composite of Mn 3d states. Due to Mn 3d with N 2p hybridization, the bandwidth of Mn 3d becomes wide so that the system behaves as an itinerant electron system. For $Mn_3Cu_{1-x}Ge_xN$ $x = 0.125, 0.25$ (see figures 4(b) and (c)), Ge 4p mainly couples with Mn 3d at −5 to −3 eV. With Ge doping increase, the DOS values of Cu 4s decrease while Ge 4p hybridizing with Mn 3d increase.

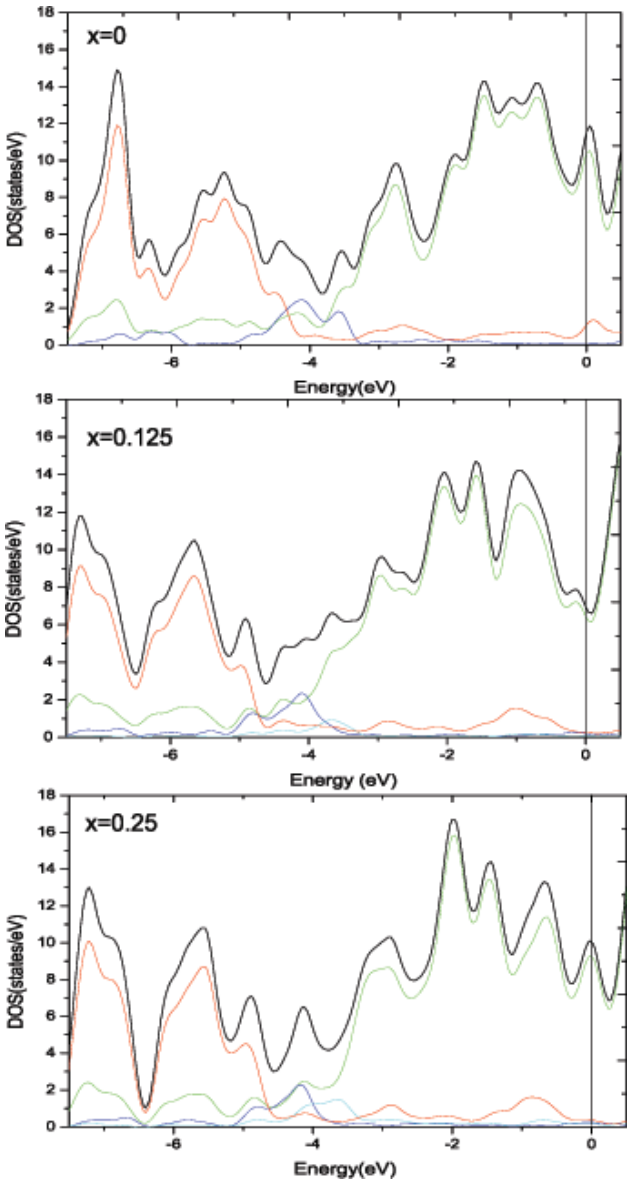

Figure 4. Total densities of states (black line) and partial densities of states of Mn 3d (green line), Cu 4s (blue line), N 2p (red line), and Ge 4p (cyan line) in $Mn_3Cu_{1-x}Ge_xN$. The energy zero is taken at the Fermi level.

The correlation from the FM state to Γ^{5g} AFM structure with Ge doping can be explained in terms of Ge 4p orbital hybridization. We know that the Cu 4s electron is itinerant in the $Mn_3Cu_{1-x}Ge_xN$ system and magnetic interaction with Mn 3d is negligible. However, Ge 4p can hybridize with Mn 3d like N 2p with Mn 3d. So we can deduce that 12 nearest-neighbor Mn of Ge are all 180° Mn–Ge–Mn FM interactions and Mn moments of 180° Mn–Ge–Mn are spin parallel configurations. Thus it just strengthens the near-neighbor Mn–Mn triangular AFM structure, where Mn moments point 120° away from each other, as shown in figure 3(c). So Ge doping can enhance the magnetic transition in the $Mn_3Cu_{1-x}Ge_xN$ system. From the DOS character of $Mn_3Cu_{1-x}Ge_xN$ ($x = 0$–0.25), we can readily argue that the coupling interaction of Ge 4p with Mn 3d increases and the Mn moments of 180° Mn–Ge–Mn are spin parallel which strengthens the Mn–Mn triangular AFM structure. When $x = 0.125$, the compound undergoes magnetic transition from the FM state to the AFM state which means that Ge 4p coupling with Mn 3d is the main reason for the magnetic transition of $Mn_3Cu_{1-x}Ge_xN$.

Table 2. Sites show Cu($x = 0$)/Ge($x = 0.125, 0.25$) atom nearest-neighbor Mn, the third and fourth columns give the nearest and next-nearest number of N, Mn, Cu, or Ge neighbors. The last column gives the magnetic moment at various sites.

				Magnetic moment (μ_B)			
x	Sites	nn	nnn	x	y	z	Total
0	Mn1	2N	4Mn + 4Cu	−2.41	−2.42	0.18	3.41
	Mn4	2N	4Mn + 4Cu	−2.41	−2.42	0.18	3.41
	Mn5	2N	4Mn + 4Cu	−2.41	2.42	0.18	3.41
	Mn6	2N	4Mn + 4Cu	−2.41	2.42	0.18	3.41
	Mn2	2N	4Mn + 4Cu	2.41	−2.42	0.19	3.42
	Mn7	2N	4Mn + 4Cu	2.41	−2.42	0.19	3.42
	Mn8	2N	4Mn + 4Cu	2.41	2.42	0.19	3.42
	Mn9	2N	4Mn + 4Cu	2.41	2.42	0.19	3.42
	Mn3	2N	4Mn + 4Cu	0.00	0.00	3.40	3.40
	Mn10	2N	4Mn + 4Cu	0.00	0.00	3.40	3.40
	Mn11	2N	4Mn + 4Cu	0.00	0.00	3.40	3.40
	Mn12	2N	4Mn + 4Cu	0.00	0.00	3.40	3.40
0.125	Mn1	2N	4Mn + 3Cu + 1Ge	1.89	0.00	−1.89	2.67
	Mn4	2N	4Mn + 3Cu + 1Ge	1.89	0.00	−1.89	2.67
	Mn5	2N	4Mn + 3Cu + 1Ge	1.89	0.00	−1.89	2.67
	Mn6	2N	4Mn + 3Cu + 1Ge	1.89	0.00	−1.89	2.67
	Mn2	2N	4Mn + 3Cu + 1Ge	0.00	−1.89	1.89	2.67
	Mn7	2N	4Mn + 3Cu + 1Ge	0.00	−1.89	1.89	2.67
	Mn8	2N	4Mn + 3Cu + 1Ge	0.00	−1.89	1.89	2.67
	Mn9	2N	4Mn + 3Cu + 1Ge	0.00	−1.89	1.89	2.67
	Mn3	2N	4Mn + 3Cu + 1Ge	−1.89	1.89	0.00	2.67
	Mn10	2N	4Mn + 3Cu + 1Ge	−1.89	1.89	0.00	2.67
	Mn11	2N	4Mn + 3Cu + 1Ge	−1.89	1.89	0.00	2.67
	Mn12	2N	4Mn + 3Cu + 1Ge	−1.89	1.89	0.00	2.67
0.25	Mn1	2N	4Mn + 2Cu + 2Ge	1.83	0.00	−1.83	2.59
	Mn4	2N	4Mn + 2Cu + 2Ge	1.83	0.00	−1.83	2.59
	Mn5	2N	4Mn + 2Cu + 2Ge	1.83	0.00	−1.83	2.59
	Mn6	2N	4Mn + 2Cu + 2Ge	1.83	0.00	−1.83	2.59
	Mn2	2N	4Mn + 3Cu + 1Ge	0.00	−1.83	1.83	2.59
	Mn7	2N	4Mn + 3Cu + 1Ge	0.00	−1.83	1.83	2.59
	Mn8	2N	4Mn + 3Cu + 1Ge	0.00	−1.83	1.83	2.59
	Mn9	2N	4Mn + 3Cu + 1Ge	0.00	−1.83	1.83	2.59
	Mn3	2N	4Mn + 2Cu + 2Ge	−1.83	1.83	0.00	2.59
	Mn10	2N	4Mn + 2Cu + 2Ge	−1.83	1.83	0.00	2.59
	Mn11	2N	4Mn + 2Cu + 2Ge	−1.83	1.83	0.00	2.59
	Mn12	2N	4Mn + 2Cu + 2Ge	−1.83	1.83	0.00	2.59

3.3. Magnetic properties

Table 2 shows the magnetic moments of Mn1–Mn12 (labeled in figure 2) and the number of near-neighbor atoms. It is found in Mn_3CuN ($x = 0$) that the Mn moments of Mn1, Mn4, Mn5, Mn6, Mn2, Mn7, Mn8, Mn9 along the x y axis are frustrated while along the z axis they are parallel. The average moment is 3.41 μ_B (experimental value 3.46 μ_B [14]). For $x = 0.125$, 0.25, the magnetic moments of Mn1–Mn12 are frustrated along the x, y, z axis and the total moment is 0.00 μ_B which is in agreement with the AFM state in experiment. We notice that the total magnetic moment of the Mn atom decreases with x increasing. It may be explained that by the increasing of Ge doping Ge 4p valence electrons fill in the band of Mn 3d and

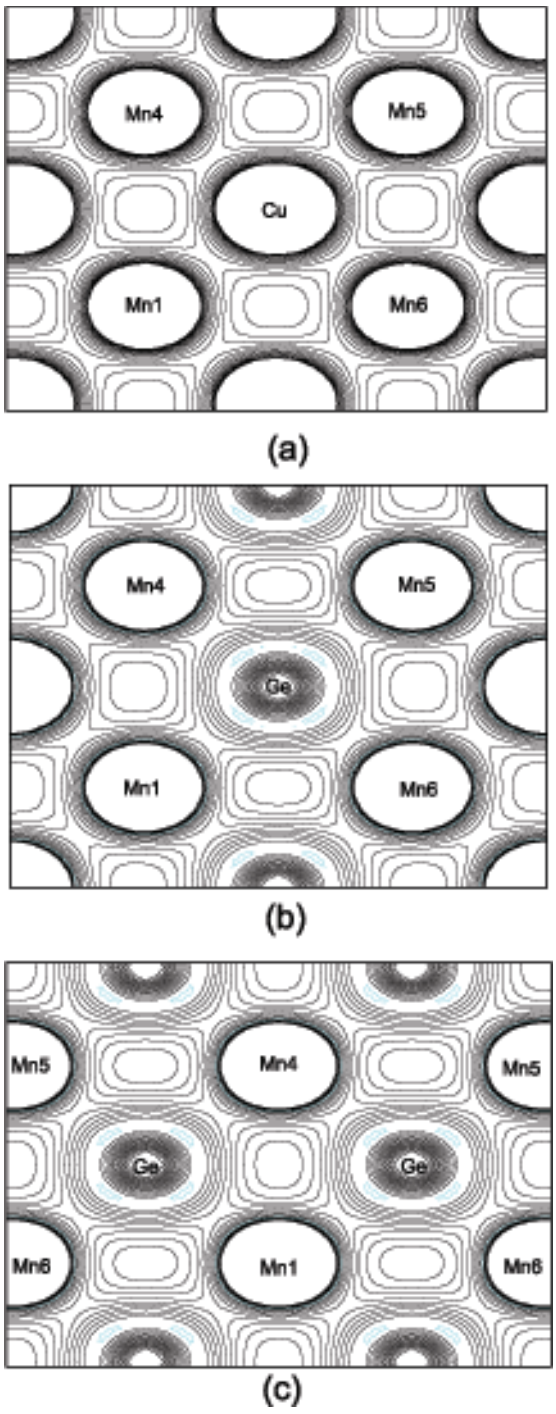

Figure 5. Contour plot of the charge density in the [020] plane for $Mn_3Cu_{1-x}Ge_xN$ at (a) $x = 0$, (b) $x = 0.125$, and (c) $x = 0.25$ (Ge 4p state labeled with a cyan line).

pair with some Mn 3d electrons. Unpaired Mn 3d electrons decrease and Mn moments decrease.

Figure 5 shows the charge density in the [020] plane for $Mn_3Cu_{1-x}Ge_xN$ at (a) $x = 0$, (b) $x = 0.125$, and (c) $x = 0.25$. From figures 5(a) and (b), we can clearly see that with the Ge doping, Ge 4p electrons hybridize with Mn 3d emergence and 180° Mn–Ge–Mn FM interactions are produced. Thus just strengthens the Mn–Mn triangular AFM structure. So Ge doping enhances the magnetic transition.

4. Conclusions

In conclusion, we have investigated the structural, electronic, and magnetic properties of $Mn_3Cu_{1-x}Ge_xN$ ($x = 0$, 0.125, 0.25) using first-principles density-functional theory within the generalized gradient approximation (GGA) + U schemes. The crystal structure of the compounds has a tetragonal lattice for $x = 0$ while it has a cubic lattice for $x = 0.125$, 0.25. The unit cell volume increases as the Ge doping increases. Our GGA + U calculations give a metallic ground state from $x = 0$ to 0.25 in $Mn_3Cu_{1-x}Ge_xN$ which is in agreement with experiments. The magnetic structure for $x = 0$ is found to be the FM state while for $x = 0.125$, 0.25 is the AFM state. From the DOS the coupling between Ge 4p with Mn 3d is the main reason for magnetic transition in $Mn_3Cu_{1-x}Ge_xN$.

Acknowledgment

Numerical calculation was carried out using the facilities of the Department of Physics in Nanjing Normal University.

References

[1] Sleight A W 1998 *Inorg. Chem.* **37** 2854
[2] Evans J S O 1999 *J. Chem. Soc. Dalton Trans.* 3317
[3] Barrera G D, Bruno J A O, Barron T H K and Allan N L 2005 *J. Phys.: Condens. Matter* **17** R217
[4] Sakamoto A, Matano T and Takeuchi H 2000 *IEICE Trans. Electron.* **E83C** 1441
[5] Kintaka K, Nishii J, Kawamoto Y, Sakamoto A and Kazansky P G 2002 *Opt. Lett.* **27** 1394
[6] Guillaume C E 1897 *C. R. Acad. Sci., Paris* **125** 235
[7] Fruchart D and Bertaut E F 1978 *J. Phys. Soc. Japan* **44** 781
[8] l'Heritier Ph, Boursier D, Fruchart R and Fruchart D 1979 *Mater. Res. Bull.* **14** 1203
[9] Fruchart R, Madar R, Barberon M, Fruchart E and Lorthioir M G 1971 *J. Physique* **32** 982
[10] Fruchart D, Bertaut E F, Madar R, Lorthioir G and Fruchart R 1971 *Solid State Commun.* **9** 1793
[11] Takenaka K and Takagi H 2005 *Appl. Phys. Lett.* **87** 261902
[12] Cross L E 1994 *Ferroelectrics* **151** 305
[13] Kimura T, Tomioka Y, Kumai R, Okimoto Y and Tokura Y 1999 *Phys. Rev. Lett.* **83** 3940
[14] Iikubo S, Kodama K, Takenaka K, Takagi H and Shamoto S 2008 *Phys. Rev.* B **77** 020409
[15] Kresse G and Hafner J 1993 *Phys. Rev.* B **47** R558
[16] Kresse G and Hafner J 1994 *Phys. Rev.* B **49** 14251
[17] Kresse G and Furthmller J 1996 *Comput. Mater. Sci.* **6** 15
[18] Kresse G and Furthmller J 1996 *Phys. Rev.* B **54** 11169
[19] Kresse G and Joubert D 1999 *Phys. Rev.* B **59** 1758
[20] Blöchl P E 1994 *Phys. Rev.* B **50** 17953
[21] Perdew J P and Wang Y 1992 *Phys. Rev.* B **45** 13244
[22] Anisimov V I, Zaanen J and Andersen O K 1991 *Phys. Rev.* B **44** 943
[23] Rohrbach A, Hafner J and Kresse G 2003 *J. Phys.: Condens. Matter* **15** 979
[24] Liechtenstein A I, Anisimov V I and Zaanen J 1995 *Phys. Rev.* B **52** R5467
[25] Dudarev S L, Botton G A, Savrasov S Y, Humphreys C J and Stutton A P 1998 *Phys. Rev.* B **57** 1505
[26] Monkhorst H J and Pack J D 1976 *Phys. Rev.* B **13** 5188
[27] Chi E O, Kim W S and Hur N H 2001 *Solid State Commun.* **120** 307–10
[28] Goodenough J B 1963 *Magnetism and the Chemical Bond* (New York: Interscience)